Recent observation of anomalous superconducting behavior of ultrathin YBCO films and single crystals of cluster borides

V.A. Gasparov

Institute of Solid State Physics RAS, Chernogolovka 142432, Moscow Region, Russia
E-mail: vgasparo@issp.ac.ru

We report the number of deviations from conventional behavior in superconducting properties of ultrathin (1−3 unit-cell (UC)) $YBa_2Cu_3O_{7-x}$ films sandwiched between semiconducting $Pr_{0.6}Y_{0.4}Ba_2Cu_3O_{7-x}$ layers and for single crystals of cluster superconductor: dodecaboride ZrB_{12}. We have found a quadratic temperature dependence of the kinetic inductance, $L_k^{-1}(T)$, at low temperatures independent of frequency, with a break in slope at T_{BKT}^{dc}, the maximum of real part of conductance, $\omega\sigma_1(T)$, and a large shift of the break temperature and the maximum position to higher temperatures with increasing frequency ω. We obtain from these data the universal ratio $T_{BKT}^{dc} / L_k^{-1}(T_{BKT}^{dc}) = 25$, 25, and 17 nHK for 1-, 2- and 3-UC films, respectively in close agreement with theoretical prediction for vortex−antivortex unbinding transition. Superfluid density of ZrB_{12} displays unconventional temperature dependence with pronounced shoulder at T/T_c equal to 0.65. Contrary to conventional theories we found a linear temperature dependence of $H_{c2}(T)$ from T_c down to 0.35 K. We suggest that both $\lambda(T)$ and $H_{c2}(T)$ dependencies can be explained by a two band BCS model with different superconducting gap and T_c.

PACS: 74.25.Nf, 74.72.Bk, 74.70.Ad, 72.15.Gd

Keywords: YBCO films, dodecaboride ZrB_{12}, inductance, penetration depth, two band superconductions.

1. Introduction

The unusual superconducting behavior of high-T_c superconductors has stimulated efforts to test whether two-dimensional (2D) behavior is an essential aspect of these materials. The question of whether an isolated unit-cell thick layer could exhibit superconductivity and how his properties relate with bulk materials remain controversial. From other side, it has been suggested from Berezinskii−Kosterlitz−Thouless (BKT) theory that there exist bound pairs of thermally excited vortices and antivortices (with opposite circulation) in 2D layers below the T_{BKT} and dissociated on free vortices and antivortices above [1,2]. Although many observations of the BKT transition in YBCO, BiSrCaCuO, and TlBaCaCuO compounds have been reported (see [3] and references therein), detailed comparison of the experimental data with the theory by Davis et al. [4] showed disagreements possibly due to inhomogeneity and vortex pinning. Rogers et al. reported that the usual BKT transition, i.e., all thermally activated vortices form vortex−antivortex pairs at temperatures below T_{BKT}, was not observed in ultrathin $Bi_2Sr_2Cu_2O_8$ films from a low-frequency noise measurement due to vortex pinning [5]. Repaci et al. [6] showed from the study of dc $I−V$ curves that free vortices exist at low temperatures even in one-unit-cell-thick YBCO films, indicating the absence of the dc BKT transition. The binding energy between a vortex−antivortex pair $U(r) \propto 1/r$ at $r > \lambda_{eff}$ (here $\lambda_{eff} = 2\lambda^2/d$ is the effective penetration depth and d is the film thickness), diverges at high distances r. Thus they had pointed out that a precondition [7] for the BKT transition to occur in a superconductor, i.e., the sample size $L_s < \lambda_{eff}$, is not satisfied even in YBCO films as thin as one unit cell.

According to the BKT theory extended to finite frequencies [8−10], higher frequency currents sense

vortex−antivortex pairs of smaller separations. At high frequency, the electromagnetic response of a $2D$ superconductor is dominated by those bound pairs that have $r \propto l_\omega$, where $l_\omega = (14D/\omega)^{1/2}$ is the vortex diffusion length and D is the vortex diffusion constant. Using the Bardeen−Stephen formula for free vortices [11], we estimate that $l_\omega < 1$ μm at $\omega > 10$ MHz, which is much less than $\lambda_{\text{eff}} = 40$ μm for the 1-UC YBCO film [3]. This implies that it is possible to detect the response of vortex−antivortex pairs with short separation lengths at high frequencies in the samples even though the usual BKT transition is not present as shown in dc and low-frequency measurements.

From other side, the recent discovery of superconductivity in magnesium diboride [12] has initiated a substantial interest in potential «high−temperature» superconducting transition in other borides (see references in Refs. 13−16). Yet, only nonstoichiometric boride compounds ($MoB_{2.5}$, $NbB_{2.5}$, Mo_2B, W_2B, $BeB_{2.75}$) demonstrate such transition. A potential clue to this contradiction may lay in the crystal structure of boron compounds, in particular in their cluster structure. Although it is widely accepted that the layered structure is crucial for high-T_c superconductivity, one can argue that clusters of light atoms are important for high T_c as well. In particular, there are a number of rather high-T_c superconductors among three-dimensional cluster compounds. Those are alkali metal doped C_{60} compounds (fullerides) Me_3C_{60} (Me = K, Na, Rb, Cs) with the highest T_c up to 33 K for $RbCs_2C_{60}$ [17,18]. It is also known that boron atoms form clusters. These are octahedral B_6 clusters in MeB_6, icosahedral B_{12} clusters in β-rhombohedral boron, and cubo-octahedral B_{12} clusters in MeB_{12}.

The quest for superconductivity in these cluster compounds has a long history. Several superconducting cubic hexaborides, MeB_6, and dodecaborides, MeB_{12}, have been discovered by Matthias et al. back in late 1960's [19] (Me = Sc, Y, Zr, La, Lu, Th). Many other cluster borides (Me = Ce, Pr, Nd, Eu, Gd, Tb, Dy, Ho, Er, Tm) were found to be ferromagnetic or antiferromagnetic [19,20]. It was suggested that the superconductivity in YB_6 and ZrB_{12} (T_c of 7.1 and 6.03 K, respectively) is exactly due to the effect of a cluster of light boron atoms. Clearly a systematic study of ZrB_{12} is needed to address the question of superconductivity in this compound.

This has been the motivation for current systematic study of the temperature dependencies of the frequency and temperature dependences of the complex sheet conductance, $\sigma(\omega,T)$, of 1-UC to 3-UC thick YBCO films sandwiched between semiconducting $Pr_{0.6}Y_{0.4}Ba_2Cu_3O_{7-x}$ layers in a frequency range bet-ween 1 MHz to 30 GHz, as well as $\lambda(T)$ and upper critical magnetic field, $H_{c2}(T)$, in single crystals of ZrB_{12}. We found a large increase of the transition temperature as a function of frequency for those films from 4 MHz to 30 GHz. We observe unusual superconducting properties of ZrB_{12} and argue that these results can be reconciled by two-band superconductivity with different T_c. Currently these data were published in Refs. 3, 16, here we present most important results of these studies.

2. Experimental setup

Ultrathin YBCO layers sandwiched between 100 Å buffer and 150 Å cover layers of $Pr_{0.6}Y_{0.4}Ba_2Cu_3O_{7-x}$ were grown epitaxially on atomically flat and well-lattice-matched (100) $LaAlO_3$ substrates using a multitarget pulsed-laser deposition (PLD) system [3]. For few UC thick films and the substrate used, the thicknesses are below the critical value for forming islands and the growth is in the range of layer by layer Stranski−Krastanov growth. The sample thickness is rather uniform due to the nature of the growth mode as characterized by using cross sectional transmission electron microscopy (TEM), atomic force microscope (AFM) and in situ RHEED. The three films thickness we examined were nominally 1-, 2-, and 3-UC thick and had the c axis normal to the film surface. The samples were made at different oxygen composition and therefore we will call them as $S1$ and $S2$ ones. The contacts were made at the edges of the 1×1 cm 3UC film for van der Pauw four-point resistance measurements.

Under ambient conditions, dodecaboride ZrB_{12} crystallizes in the *fcc* structure of the UB_{12} type [15,16]. In this structure, the Zr atoms are located at interstitial openings among the close-packed B_{12} clusters. Our ZrB_{12} single crystals were grown using a floating-zone method [14]. The obtained single crystal ingots had a typical diameter of about 5 to 6 mm and a length of 40 mm. To assure good quality of our samples we performed metallographic and x-ray investigations of as grown ingots. We discovered that most parts of the ZrB_{12} ingot contained a needle like phase of nonsuperconducting ZrB_2. We believe that ZrB_2 needles are due to preparation of ZrB_{12} single crystals from a mixture of a certain amount of ZrB_2 and an excess of boron [14]. We believe that unconventional properties observed from other studies may be due to these sample problems [16]. Therefore, special care has been taken to cut the samples from ZrB_2 phase free parts.

We used the spark erosion method to cut the single crystal ingots into rectangular <100> oriented bars of about 0.5×0.5×8 mm. The samples were lapped with

diamond paste and etched in hot nitrogen acid to remove any damage induced by lapping deteriorated surface layers. A well-defined geometry of the samples provided for the precise $\rho(T)$ and superconducting properties measurements. Temperature was measured with platinum (PT-103) and carbon glass (CGR-1-500) sensors. Magnetic measurements of $\rho(T,H)$ and $\lambda(T,H)$ were carried out using a superconducting coil in applied fields of up to 6 T down to 1.3 K. Additional dc and ac $\rho(H)$ measurements were performed in the National High Magnetic Field Laboratory in Tallahassee, Florida (NHMFL) at temperatures down to 0.35 K. The dc magnetic field was applied in the direction of the current flow.

For this study, two highly crystalline, superconducting films of MgB_2 were grown on an *r*-plane sapphire substrate in a two-step process [22]. Deposition of boron precursor films via electron-beam evaporation was followed by *ex situ* postannealing at 890 °C in the presence of bulk MgB_2 and Mg vapor. We investigated films of 500 and 700 nm thickness with corresponding T_{c0}'s of 38 K and 39.2 K, respectively. The details of the preparation technique are described elsewhere [22].

The $\sigma(\omega,T)$ at RF in thin 1–3 UC YBCO and MgB_2 films was investigated employing a single coil mutual inductance technique. This technique, originally proposed in Ref. 23 and lately improved in Ref. 24, has the advantages of the well known two-coil geometry, and was extensively used for the study of the $\lambda(T)$ dependence for YBCO and MgB_2 films [3,15,16]. In this radio frequency technique, the change of inductance ΔL of a one-layer pancake coil located in the proximity of the film and connected in parallel with a capacitor C is measured. The LC circuit is driven by the impedance meter (VM-508 TESLA) operating at 2–50 MHz, with a high frequency stability of 10 Hz. The film is placed at small distance (≈ 0.1 mm) below the coil. Both sample and coil are in a vacuum, but the coil holder is thermally connected with helium bath, while the sample holder is isolated and may be heated. During the experiment the coil was kept at 2.5 K, whereas the sample temperature was varied from 4.2 up to 100 K. Such design allows us to eliminate possible effects in temperature changes in L and C on the measurements.

The complex mutual inductance M between the coil and the film can be obtained through

$$\text{Re } M(T) = L_0 \left(\frac{f_0^2}{f^2(T)} - 1 \right), \qquad (1)$$

$$\text{Im } M(T) = \frac{1}{2\pi f(T)C^2} \left[\frac{1}{Z(T)} - \frac{1}{Z_0(T)} \frac{f^2(T)}{f_0^2} \right]. \qquad (2)$$

Here L, $Z(T)$, $f(T)$, L_0, Z_0 and f_0 are the inductance, impedance and the resonant frequency of the circuit with and without the sample, respectively. In the low frequency regime, where the coil wire diameter is much thinner than the skin depth at the working frequency, the expression of the variation of the $M(T)$ (relative to the case where no sample is in the coil, M_0), as a function of the $\lambda(T)$ may written as [24]:

$$\Delta M(T) = \pi\mu_0 \int_0^\infty \frac{M(q)}{1 + 2ql \coth\left(\dfrac{d}{l}\right)} dq , \qquad (3)$$

where $M(q)$ plays the role of mutual inductance at a given wave number q in the film plane and depends on the sample-coil distance h, d is the sample thickness, and l is a complex length defined as $l = [1/(i\omega\mu_0\sigma_1+\lambda^2)]^{1/2}$, (more details can be found in Refs. 16, 24). A change in real, Re $M(T)$, and imaginary, Im $M(T)$, parts of $M(T)$ were detected as a change of resonant frequency $f(T)$ of the oscillating signal and impedance $Z(T)$ of the LC circuit, and converted into $L_k(T)$ and $\sigma_1(T)$ by both, using Eqs. (1), (2) with inversion mathematical procedure and Eq. (3).

The high frequency (100 MHz–1 GHz) measurements were performed using the cavity formed with a similar spiral coil with no capacity in parallel. The coil form the radio frequency resonator coupled to a two coupling loops and is driven by the radio-frequency signal generator/receiver. In this case the quality factor of the resonator Q and the resonance frequency were measured and converted to Re $M(T)$ by Eq. (1) and to Im $M(T)$ by:

$$\text{Im } M(T) = L_0 \frac{f_0}{f(T)} \left[\frac{1}{Q(T)} \frac{f_0}{f(T)} - \frac{1}{Q_0} \right], \qquad (4)$$

where $Q(T)$ and $Q_0(T)$ are the quality factors with and without the samples, respectively.

The MW losses were measured using a resonant cavity technique with the gold-plated copper cylindrical cavity operated in the TE_{011} mode at 29.9 GHz. The samples were mounted as a part of the bottom of the cavity through a thin gold-plated Cu-diaphragm with a small central hole so that the sample itself occupies only the holes part of the endplate through a transparent Teflon film. The resonator was operating in a transmission configuration. During the experimental run, we measured the amplitude of the transmitted signal at resonance as a function of tem-

perature. The resonator was coupled weakly to the input and output waveguides so the amplitude of the transmitted signal at resonance is proportional to the square of unloaded quality Q. We assume the MW electric field E in the film to be uniform along normal direction and equal to the E without the film. The $\sigma_1(\omega, T)$ is thus proportional to $\Delta Q^{-1}(T) = Q^{-1}(T) - Q_0^{-1}(T)$, where $Q(T)$ and $Q_0(T)$ are the quality factors with and without the samples, respectively.

We used similar radio frequency LC technique [15,16,25] to measure $\lambda(T)$ of ZrB_{12} samples. This technique employs a rectangular solenoid coil into which the sample is placed rather then use of spiral coil. The connection between parameters of the circuit and $\lambda(T)$ is described by following equation:

$$\lambda(T) - \lambda(0) = \delta \frac{f^{-2}(T) - f^{-2}(0)}{f^{-2}(T_c) - f^{-2}(0)} . \quad (5)$$

Here $\delta = 0.5(c^2\rho / 2\pi\omega)^{1/2}$ is the imaginary part of a skin depth above T_c, which was determined from the $\rho(T)$ measurements close to T_c, $f(T)$ is the resonance frequency of the circuit at arbitrary T and $f(T_c)$ and $f(0)$ are the resonance frequency of the circuit at the superconducting transition and at zero temperature, respectively.

3. Magnetic penetration depth in YBCO films

Figure 1 displays the Re $M(T)$ and Im $M(T)$ curves for a 2UC S2 film at three different frequencies from 3 MHz to 500 MHz as measured by different techniques: LC circuit and spiral coil resonator. The HF data are normalized to RF Re $M(0)$ data because of different gap h values used. The most noticeable feature of these data is rather high shift of the onset point T_{c0} of Re $M(T)$ transition with frequency, not observed in such measurements on thick films. Notice also, that the inductive response, Re $M(T)$, starts at lower temperatures than Im $M(T)$, characterized by a peak close to transition, and this shift is raised with frequency. We have carried out the mutual inductance measurements on $Pr_{0.6}Y_{0.4}Ba_2Cu_3O_{7-x}$ films and observed no any features in the temperature dependences of the mutual inductance $M(T)$.

The Re $M(T)$ and Im $M(T)$ data are converted to $L_k^{-1}(T)$ and Re $\sigma(T)$ using Eq. (3) and the mathematical inversion procedure [3] based on the same approach as in the two-coil mutual inductance method. Figure 2 shows the $L_k^{-1}(T)$ curves in very low perpendicular magnetic fields, and zero field ωRe $\sigma(T)$ for the 1-UC and 2-UC films (S1). We found that $L_k^{-1}(T)$ fit well over a wide temperature range by a parabolic dependence: $L_k^{-1}(T) = L_k^{-1}(0)[1 - (T/T_{c0})^2]$, shown as thin solid lines in Fig. 2. We emphasize that this qua-
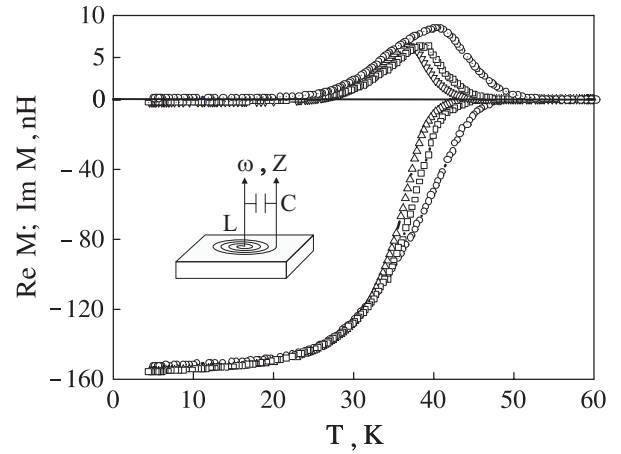

Fig. 1. The Re $M(T)$ and Im $M(T)$ curves for a 2-UC film (S2) at different frequencies, MHz: 3 (triangles), 26 (squares) and 500 (circles) calculated from raw $f(T)$, $Z(T)$ and $Q(T)$ data. The solid lines describe a guide for the eye. Inset shows experimental set-up.

dratics equation fit the data below characteristic temperature which we define as T_{BKT}^{dc}, and which is below the positions of the peaks in ωRe $\sigma(T)$, which we define as T_{BKT}^{ω}. The mean field transition temperature, T_{c0}, determined by extrapolation of $L_k^{-1}(T)$ to 0, is larger than the onset of transitions of $L_k^{-1}(T)$, while is close to the onset point of ωRe $\sigma(T)$ curves. Also, the $L_k^{-1}(0)$ fitted data are the same for $H = 0$ and 5 mT while have different T_{c0}.

In Fig. 3, we plot ωRe $\sigma(T)$ at 8 MHz and $\Delta Q^{-1}(T)/Q_0^{-1}(4.2$ K) determined from MW data (30 GHz) for 3-UC sample (S1). The dc resistive transition of the same sample is also shown in the figure. According to the Coulomb gas scaling model, the re-
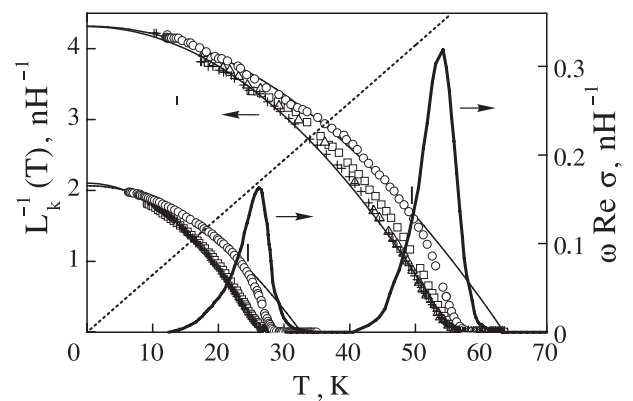

Fig. 2. Temperature dependence of $L_k^{-1}(T)$ for 1- and 2-UC films (S1) at 8 MHz and different magnetic fields, mT: 0 (circles), 2 (squares), 3 (triangles) and 4 (crosses). The solid lines curves shows ωRe $\sigma(T)$ at zero field. The thin solid lines are quadratic fits to $L_k^{-1}(T)$ below T_{BKT}^{dc} and for magnetic field data. Also shown is the theoretical BKT function (dashed line).

sistance ratio R/R_n is proportional to the number of free vortices and should follow a universal function of an effective temperature scaling variable $X = T(T_{c0} - T_{BKT}^{dc})/T_{BKT}^{dc}(T_{c0} - T)$ [8], which can be approximated by $\rho/\rho_n = C_0 X \exp[-C_1(X-1)^{-1/2}]$ (here ρ_n is the normal state resistivity, $C_0 = 1.7$ and $C_1 = 4.9$ are constants). We plot $T/X(T)$ as a function of T obtained by fitting ρ/ρ_n data for the 3-UC film with this equation in the inset of Fig. 3. The best fit was found with $T_{c0} = 78.5$ K (the point where $T/X = 0$) and $T_{BKT}^{dc} = 56$ K. Here T_{BKT}^{dc} represents a nominal dc BKT transition temperature which is lower then T_{BKT}^{ω} determined from RF and MW data.

There are three major features observed in our RF and MW measurements: (i) the large frequency dependence of $T_c(\omega)$, (ii) a foot jump in temperature dependence of the $L_k^{-1}(T)$, which is destroyed in weak magnetic fields, and (iii) a maximum in $\omega \mathrm{Re}\, \sigma(T)$ with the onset of transition at higher temperatures than that of the $L_k^{-1}(T)$.

Indeed, as we can see from Fig. 1, the T_{BKT}^{ω} value, determined as the maximum position of losses, increases on 4 K (from 36.6 to 40.7 K) as the frequency raise from 3 to 500 MHz for 2-UC YBCO S2 film. The T_{BKT}^{ω} value shift at 30 GHz is much larger: 74 K as compared with 61.5 K at 8 MHz (see Fig. 3). Even larger shift of T_{BKT}^{ω} was observed in 1-UC film and no shift was detected in a 2000 Å thick YBCO film.

We determined the T_{BKT}^{ω} as the peak position of $\sigma_1(T)$ point. We also used the T_{BKT}^{dc} as the point where $L_k^{-1}(T)$ deviates from the square fit (see Fig. 2), as was used by Hebard et al. [30]. The ratio $T_{BKT}^{dc}/L_k^{-1}(T_{BKT}^{dc})$ thus equal to 25, 25, and 17 nHK for 1-, 2- and 3-UC S1 films, respectively, is about
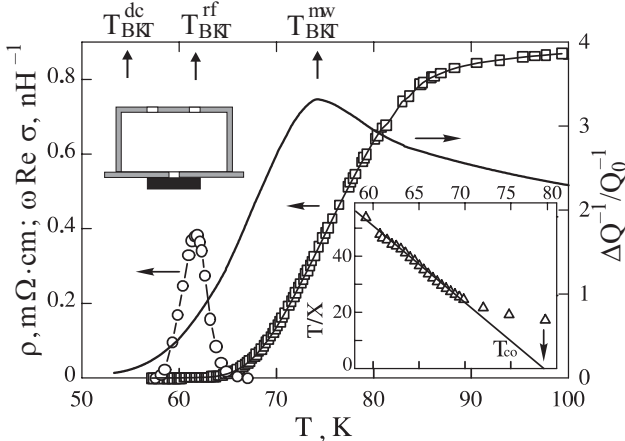
constant, which however is larger than the theoretical estimation $T_{BKT}^{dc}\lambda^2(T_{BKT}^{dc})/d = \phi_0^2/32\pi^2 k_B = 0.98$ cm·K (or $T_{BKT}^{dc}/L_k^{-1}(T_{BKT}^{dc}) = 12.3$ nHK) [31] ignoring small dynamic theory corrections of Ambegaokar et al. [9] to the renormalized coupling constant K_R.

In order to see whether this assumption is correct, we plot theoretical BKT function $L_k^{-1}(T)$ as dashed straight line on Fig. 2 derived from the universal relationship:

$$K_R = \frac{d}{\lambda^2}\frac{\hbar^2 c^2}{16\pi e^2 k_B T_{BKT}} = \frac{2}{\pi} \qquad (6)$$

predicted by theory [4]. Notice however, that this theoretical dependence is valid for dc case, while the frequency dependence of T_{BKT}^{ω} is obvious from the picture discussed above. This is why the critical temperatures determined from the intercept of dashed theoretical line with experimental $L_k^{-1}(T)$ is lower then the peak position of $\sigma_1(T)$. To see whether this description is correct, we plot the dependence of the penetration depth $\lambda^{-2}(T)$ derived from $L_k^{-1}(T)$, versus scaling variable — normalized temperature T/T_{BKT}^{ω} on Fig. 4. It is obvious, that all data for three studied S1 films at 8 MHz fall on the same curve, which proof of our definition of T_{BKT}^{ω} as the peak position of $\sigma_1(T)$.

The Abrikosov vortex lattice parameter a_v is the scale limiting the formation of vortex−antivortex pairs in magnetic field. We can estimate the field H_{ext} which destroys the vortex pair unbinding from the following relation: $l_\omega \propto a_v = (\phi_0/H_{ext})^{1/2}$. This estimation gives $H_{ext} \approx 1.5$ mT at 10 MHz for 1-UC and 2-UC films in good agreement with the experimental results (see Fig. 2). It is generally believed that the inhomogeneity can destroy the interaction of
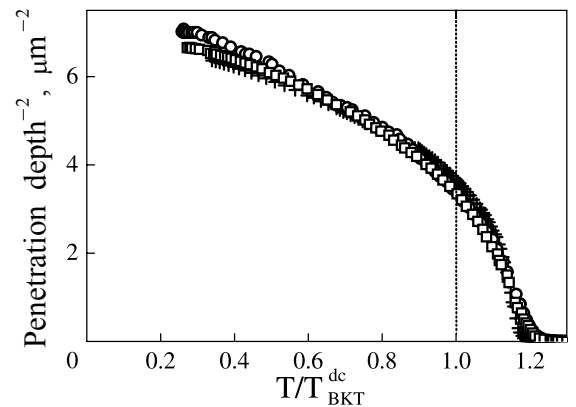

Fig. 3. Temperature dependence of dc $\rho(T)$ (squares), $\omega \mathrm{Re}\, \sigma(T)$ (circles) at 8 MHz and $\Delta Q^{-1}(T)/Q_0^{-1}(4.2$ K) at 30 GHz (solid line) for a 3-UC sample (S1). Inset shows the universal plot: T/X vs T. Arrows indicate the T_{BKT} values determined from the dc resistivity, loss function at 8 MHz and MW measurements (30 GHz).

Fig. 4. The penetration depth $\lambda^{-2}(T)$ derived from $L_k(T) = \mu_0\lambda^2/d$ vs normalized temperature T/T_{BKT}^{ω} for: 1-UC (crosses), 2-UC (squares) and 3-UC (circles) films.

vortex – antivortex pairs. However, inhomogeneity can never help to create the BKT transition.

It is easy to see from above, we report several results which are in qualitative agreement to the prediction of the dynamic theory of vortex – antivortex pairs with short separation lengths. These effects must be from intrinsic effect and can not be the result of inhomogeneity or due to the skin effect in the samples [3].

4. Magnetic penetration depth in ZrB$_{12}$

In the BCS theory the London penetration depth is identical with $\lambda(T)$ for specular and diffuse surface scattering and for negligible nonlocal effects. For a BCS-type superconductor with the conventional s-wave pairing form, the $\lambda(T)$ has an exponentially vanishing temperature dependence below $T_c/2$ (where $\Delta(T)$ is almost constant):

$$\lambda(T) = \lambda(0)\left[1 + \sqrt{\frac{\pi\Delta(0)}{2k_BT}} \, \exp\left(-\frac{\Delta(0)}{k_BT} \right) \right] \quad (7)$$

for clean limit: $l > \xi$, and

$$\lambda(T) = \lambda(0) \sqrt{\frac{1}{\tanh\left(\dfrac{\Delta(0)}{2k_BT} \right)}} \quad (8)$$

for dirty limit: $l < \xi$ [13]. Here $\Delta(0)$ is the energy gap and $\lambda(0)$ is the penetration depth at zero temperature. Close to T_c $\lambda(T)$ dependence has a BCS form [16]:

$$\lambda(T) = \frac{\lambda(0)}{\sqrt{2\left(1 - \dfrac{T}{T_c} \right)}} \, . \quad (9)$$

Important problems for $\lambda(T)$ measurements are (i) determination of basic superconducting parameter $\lambda(0)$ and (ii) temperature dependence law, to see whether s-wave or d-wave pairing forms exist. Both these problems can be addressed from low-T $\lambda(T)$ dependence according to Eqs. (7) and (8). We used Eq. (5) to extrapolate the resonance frequency $f(T)$ of our LC circuit down to zero temperature.

To address the problem with $\lambda(0)$ we plot $\lambda(T) - \lambda(0)$ data versus BCS reduced temperature: $1/\sqrt{2(1 - T/T_c)}$ in the region close to T_c (see the inset to Fig. 5). The advantage of this procedure is the insensitivity of such analysis to the choice of $f(0)$ on this temperature scale. The value of $T_c = 5.992$ K used in this data analysis is obtained by getting best linear fit of the $\lambda(T) - \lambda(0)$ vs $1/\sqrt{2(1 - T/T_c)}$ plot. Remarkably there is only a few millidegrees difference
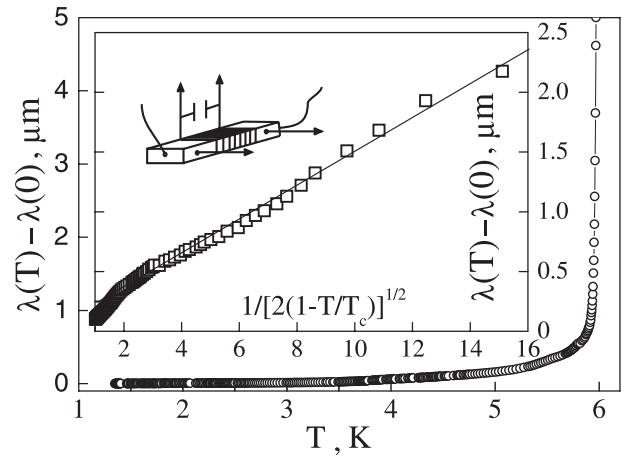

Fig. 5. Temperature variations of $\lambda(T)$ for ZrB$_{12}$ sample. The inset shows $\lambda(T) - \lambda(0)$ versus BCS reduced temperature.

between T_c obtained from the fit and actual T_{c0}. We use the slope of $\lambda(T) - \lambda(0)$ vs $1/\sqrt{2(1 - T/T_c)}$ and Eq. (9) to obtain the value of $\lambda(0) = 143$ nm.

In order to investigate the temperature dependence of $\lambda(T)$ in the whole temperature region, in Fig. 6 we plot the superfluid density $\lambda^2(0)/\lambda^2(T)$ versus the reduced T/T_c for ZrB$_{12}$ sample using this $\lambda(0)$ determined from one gap fit close to T_c. One can easily notice an unconventional behavior of superfluid density with pronounced shoulder at T/T_c equal to 0.65. This feature can be explained by a model of two independent BCS superconducting bands with different plasma frequencies, gaps and T_c's [16]. We label these two bands as p- and d-bands in accordance to electron structure of ZrB$_{12}$ [26]. It is clear from partial BCS
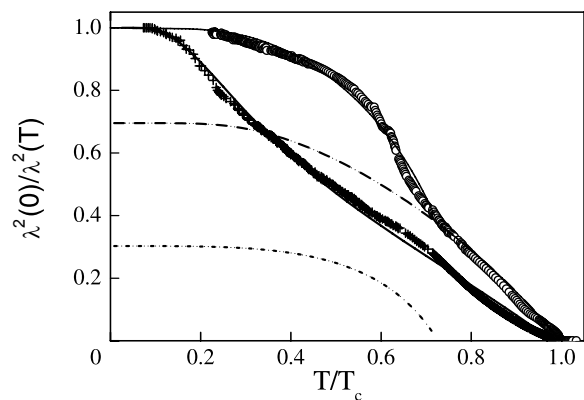

Fig. 6. Superfluid density, $[\lambda(0)/\lambda(T)]^2$, of the ZrB$_{12}$ single crystal sample and MgB$_2$ thin film (crosses). The predicted behavior of $[\lambda(0)/\lambda(T)]^2$ within the two band model as described in the text is shown by the solid, dashed (p-band) and dotted (d-band) lines. The solid line represent BCS fit of MgB$_2$ data using $2\Delta(0)/k_BT_c$ as fit parameter.

curves, that single gap BCS model is unable to fit a full $[\lambda(0)/\lambda(T)]^2$ unconventional dependence.

For a dirty limit [27] we can write for two band superconductor in:

$$\frac{1}{\lambda^2(T)} = \frac{\Delta_p(T)\tanh\left(\frac{\Delta_p}{2k_BT}\right)}{\lambda_p^2(0)\Delta_p(0)} + \frac{\Delta_d(T)\tanh\left(\frac{\Delta_d}{2k_BT}\right)}{\lambda_d^2(0)\Delta_d(0)}.$$

(10)

Here Δ_i is the superconducting energy gap and $\lambda_i(0)$ is residual penetration depth in the p- or d-band. Using this two gap $\lambda(T)$ BCS-like dependence and interpolation formula $\Delta(T) = \Delta(0)\tanh[1.88 \times (T_c/T - 1)^{1/2}]$ we fit the experimental data with six fitting parameters: λ_i, Δ_i and T_{ci}. From this fit we obtain $T_c^p = 6.0$ K, $T_c^d = 4.35$ K, $\Delta_p(0) = 0.73$ meV, $\Delta_d(0) = 1.21$ meV, $\lambda_p(0) = 170$ nm and $\lambda_d(0) = 260$ nm, for p- and d-bands, respectively. Dashed and dotted lines in Fig. 6 show the contributions of each p- and d-bands, respectively. Clearly low-temperature dependence of $\lambda^2(0)/\lambda^2(T)$ is dominated by the d-band with the smallest T_c, whereas the high-temperature behavior results from the p-band with the larger T_c. The reduced energy gap for p-band, $2\Delta_p(0)/k_BT_c^p = 2.81$, is rather small relative to the BCS value 3.52, while d-band value, $2\Delta_d(0)/k_BT_c^d = 6.44$, is twice as big. Thus we suggest that ZrB_{12} may have two superconducting bands with different T_c and order parameters. Notice that this unusual conclusion may be right for two bands in the limit of zero interband coupling in agreement with resistivity data [13]. Also, the $\Delta(0)$ of ZrB_{12} may not be constant over the Fermi surface.

We based our conclusion on the two-gap model for dirty-limit superconductors, suggested by Gurevich [27]. In this model, we can write

$$\frac{1}{\lambda^2(T)} = \frac{4\pi^2 e^2}{\hbar c^2}(N_p\Delta_p D_p + N_d\Delta_d D_d) =$$

$$= \frac{1}{\lambda_p^2(0)} + \frac{1}{\lambda_d^2(0)},$$ (11)

where N_i, Δ_i and D_i are the density of states, the energy gap and the diffusivity in p- and d-bands, respectively. It follows from electron band structure calculations that the dominant contribution to the density of states $N(E_F)$ is made by the Zr_{4d} and B_{2p} states, with $N_d = 7.3\cdot10^{21}$ st/eV·cm^3 and $N_p = 8.7\cdot10^{21}$ st/eV·cm^3, respectively [26]. The B_{2p} bonding states are responsible for the formation of B_{12} intra cluster covalent bonds. In turn, Zr_{4d} bands are due to Zr sub lattice. We use this two band approach (Eq. (10)) to obtain p-band diffusivity of

$D_p = 57$ cm^2/s and d-band diffusivity of $D_d = 17$ cm^2/s. Note that there is almost a six times difference between the p- and d-band diffusivity. We use this result for our discussion of $H_{c2}(T)$ data in the following paragraph.

The important goal of this chapter is comparison of ZrB_{12} and MgB_2 data. In Fig. 6 we show the temperature variation of a superfluid density, $\lambda^2(0)/\lambda^2(T)$, versus reduced temperature T/T_c for the best MgB_2 film as determined from the one-coil technique (Eq. (1)) and inversion procedure from Eq. (3) with $\lambda(0) = 114$ nm. The solid line represents BCS single gap calculations by the aid of a single term of Eq. (10) and using finite energy gap ($\Delta(0) = 1.93$ meV) as the fit parameter. According to Fig. 5, there is a very good agreement between experimental data and the single gap BCS curve over the full temperature range. The reduced energy gap $2\Delta(0)/k_BT_c$ is evaluated to be 1.14. It is actually within the range of values for 3D π bands obtained by PCS on MgB_2 single crystals [16]. Both $\Delta(0)$ and $\lambda(0)$ are consistent with microwave measurements on similar c-axis oriented thin films (3.2 meV and 107 nm, respectively) [28]. Notice that we studied here the penetration depth in the ab-plane due to the samples being c-axis oriented thin films. This feature predicts that our $\lambda_{ab}(T)$ is determined by the small energy gap for the π band.

5. Upper critical magnetic field

We now turn to the electronic transport data acquired in magnetic field. Figure 7 displays the
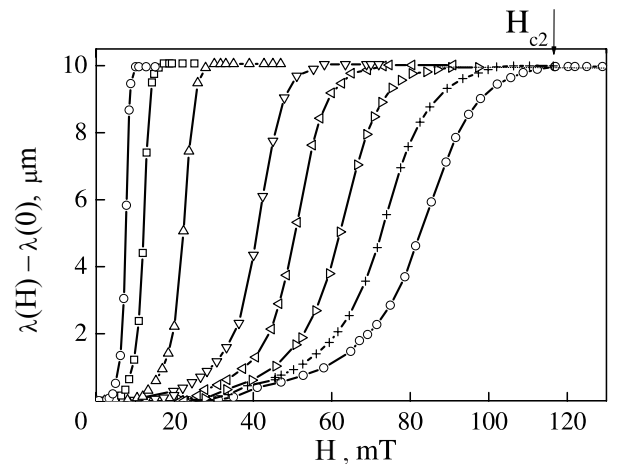
Fig. 7. Magnetic field variation of $\lambda(H)$ of a single crystal ZrB_{12} sample at different temperatures, K: 5.66, 5.53, 5.02, 4.06, 3.45, 2.84, 2.15 and 1.43, from the left to the right. The solid lines are the guides for the eye. The arrow describes how H_{c2} has been deduced.

penetration depth magnetic field transitions at various temperatures down to 1.43 K with the fields oriented along the sample bar. Figure 7 clearly demonstrates a well defined onset of $\lambda(H)$ transition. We used this onset to estimate H_{c2}. Similar approach was used to $\rho(T)$ data [16]. Figure 8 presents the H_{c2} dependence defined at the onsets of the finite $\rho(H)$ and $\lambda(H)$. Remarkable feature of this plot is an linear increase of H_{c2} with decreasing temperature down to 0.35 K.

To see whether one gap BCS model may work for ZrB_{12}, we extrapolate $H_{c2}(T)$ to zero temperature by use of the derivative of $dH_{c2}(T)/dT$ close to T_c and the assumption that the zero temperature $H_{c2}(0) = 0.69 T_c dH_{c2}/dT|_{T_c}$. The resulting $H_{c2}(0) = 114$ mT is substantially lower than the low temperature onset data below 3 K. Linear extrapolation of $H_{c2}(T)$ to $T = 0$ gives $H_{c2}(0) = 162$ mT. We used this value to obtain the coherence length $\xi(0)$, by employing the relations $H_{c2}(0) = \phi_0/2\pi\xi^2(0)$. The latter yields $\xi(0) = 45$ nm, which is substantially larger than a few angstroms coherence length of high-T_c superconductors. In contrast to Ref. 21 our estimations agree well with the Ginzburg–Landau parameter $\kappa = \lambda/\xi$. Using our values of λ_p and λ_d data we obtain $\kappa_p = 3.8$ and $\kappa_d = 5.8$. Both values of κ_d are larger then $1/\sqrt{2}$ that implies that ZrB_{12} is type II superconductor at all T. Using the GL expression for $H_{c1}(T) = \phi_0 \ln \kappa/4\pi\lambda^2$ we obtain: $H_{c2}/H_{c1} = 2\kappa^2/\ln \kappa$. From the value $H_{c2}(0)$ obtained above and the H_{c1} data from [16], we find $\kappa = 6.3$ and $\lambda(0) = 280$ nm which is in good agreement with the value $\lambda_p(0) = 260$ nm obtained from two gap BCS fit for d-band.

In contrast to the conventional BCS theory, $H_{c2}(T)$ dependence is linear over an extended temperature range with no evidence of saturation down to 0.35 K.
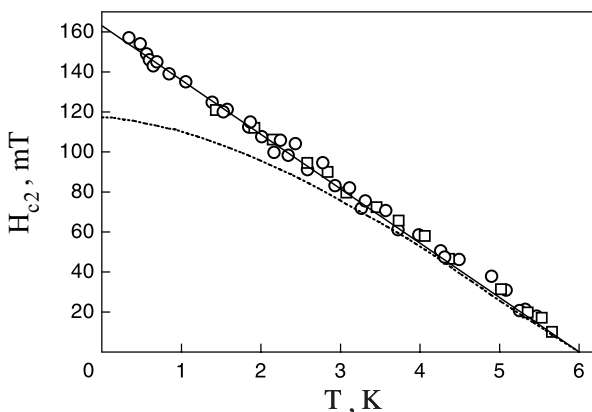
Similar linear $H_{c2}(T)$ dependence has been observed in MgB_2 (Refs. 29 and 30) and $BaNbO_x$ (Ref. 31) compounds. One can describe this behavior of upper critical field using the two-gap approach. According to Gurevich [27], the zero-temperature value of the H_{c2} is significantly enhanced in the two gap dirty limit superconductor model:

$$H_{c2}(0) = \frac{\phi_0 k_B T_c}{1.12\hbar\sqrt{D_1 D_2}} \exp\left(\frac{g}{2}\right), \qquad (12)$$

as compared to the one-gap dirty limit approximation $H_{c2}(0) = \phi_0 k_B T_c/1.12\hbar D$. Here g is a rather complicated function of the matrix of the BCS superconducting coupling constants.

In the limit of $D_2 << D_1$ we can simply approximate $g \approx |\ln (D_2/D_1)|$. The large ratio of D_2/D_1 leads to the enhancement of $H_{c2}(0)$ and results in the upward curvature of the $H_{c2}(T)$ close to $T = 0$ [27]. According to our $\lambda(T)$ data (see above), we found very different diffusivities for p- and d-bands: $D_p/D_d \approx 3$. Thus we can speculate that the limiting value of $H_{c2}(0)$ is dominated by d-band with lower diffusivity $D_d = 17$ cm^2/s, while the derivative dH_{c2}/dT close to T_c is due to larger diffusivity band ($D_p = 56$ cm^2/s). Indeed, simple estimation of $D_p = 4\phi_0 k_B/\pi^2\hbar dH_{c2}/dT = 39$ cm^2/s from derivative $dH_{c2}/dT = 0.027$ T/K close to T_c gives almost the same diffusivity relative to one estimated from $\lambda(T)$ for the p-band. Thus we believe that the two gap theoretical model qualitatively explains the unconventional linear $H_{c2}(T)$ dependence, which supports our conclusion about the two gap nature of superconductivity in ZrB_{12}.

The possibility of the multigap nature of the superconducting state was predicted for a multiband superconductor with large difference of the $e-p$ interaction at different Fermi-surface sheets (see Ref. 32 and references therein). To date MgB_2 has been the only compound with the behavior consistent with the idea of two distinct gaps with the same T_c. We believe that our data can add ZrB_{12} as another unconventional example of multi gap and multi-T_c superconductor.

Although observed two gap behavior of $\lambda^2(0)/\lambda^2(T)$ in ZrB_{12} is similar to that in high-T_c superconductors, observation of two different T_c in these bands is unconventional. This also relates to the linear $H_{c2}(T)$ dependence in the wide temperature range up to T_c. Striking two gap BCS behavior observed calls certainly for a new study of low-T energy gap and $H_{c2}(T)$ of ZrB_{12} for understand the nature of superconductivity in this cluster compounds.

Fig. 8. Temperature variations of $H_{c2}(T)$ of ZrB_{12}. Symbols: the onset $H_{c2}(T)$ data determined from $\rho(H)$ (circles) and $\lambda(H)$ (squares). Dotted line is the BCS data determined from the *HW* formula [33].

6. Conclusion

In summary, we have compared our experimental results on ultrathin YBCO films with the extended dynamic theory for BKT transition and found that the vortex−antivortex pairs with short separation lengths are present. The unbinding of the vortex pairs were observable at high frequencies even though a true BKT transition is absent in the samples. Our results also indicate that part of the transition broadening in ultrathin YBCO films can be related to the dissociation of vortex−antivortex pairs.

While the temperature dependence of $\lambda(T)$ in thin c-axis oriented thin film MgB_2 samples is well described by an isotropic s-type order parameter, we find unconventional behavior of ZrB_{12} superfluid density with pronounced shoulder at T/T_c equal to 0.65. The $H_{c2}(T)$ dependences have been deduced from the $\rho(H)$ and $\lambda(H)$ data. Both techniques reveal an unconventional linear temperature dependence of $H_{c2}(T)$. We conclude therefore that ZrB_{12} presents a evidence of the unconventional two-gap superconductivity with different T_c in the different bands.

1. V.L. Berezinskii, *ZhETF* **59**, 907 (1970); *ibid* **61**, 1144 (1971).

2. J. M. Kosterlitz and D.J. Thouless, *J. Phys.* **C6**, 1181 (1973); *Prog. Low Temp. Phys.* **B7**, 373 (1978).

3. V.A. Gasparov, G. Tsydynzhapov, I.E. Batov, and Qi Li, *J. Low Temp. Phys.* **139**, 49 (2005).

4. L.C. Davis, M.R. Beasley, and D.J. Scalapino, *Phys. Rev.* **B42**, 99 (1990).

5. C.T. Rogers, K.E. Myers, J. N. Eckstein et al., *Phys. Rev. Lett.* **69**, 160 (1992).

6. J.M. Repaci, C. Kwon, Qi Li et al., *Phys. Rev.* **B54**, 9674 (1996).

7. M.R. Beasley, J.E. Mooij, and T.P. Orlando, *Phys. Rev. Lett.* **42**, 1165 (1979).

8. P. Minnhagen, B.I. Halperin, and D.R. Nelson et al., *Phys. Rev.* **B23**, 5745 (1981); *Rev. Mod. Phys.* **59**, 1001 (1987).

9. V. Ambegaokar, B.I. Halperin, and D.R. Nelson et al., *Phys. Rev. Lett.* **40**, 783 (1978); *Phys. Rev.* **B21**, 1806 (1980).

10. B.J. Halperin and D.R. Nelson, *J. Low Temp. Phys.* **36**, 599 (1979).

11. J. Bardeen and M.J. Stephen, *Phys. Rev.* **140**, A1197 (1965).

12. J. Nagamatsu, N. Nakagawa, T. Muranaka, Y. Zanitani, and J. Akimitsu, *Nature* **410**, 63 (2001).

13. V.A. Gasparov, N.S. Sidorov, I.I. Zver'kova, and M.P. Kulakov, *Pis'ma Zh. Eksp. Teor. Fiz.* **73**, 601 (2001) [*JETP Lett.* **73**, 532 (2001)].

14. V.A. Gasparov, M.P. Kulakov, I.I. Zver'kova, N.S. Sidorov, V.B. Filipov, A.B. Lyashenko, and Yu.B. Paderno, *Pis'ma Zh. Eksp. Teor. Fiz.* **80**, 376 (2004) [*JETP* **80**, 330 (2004)].

15. V.A. Gasparov, N.S. Sidorov, I.I. Zver'kova, S.S. Khassanov, and M.P. Kulakov, *Zh. Eksp. Teor. Fiz.* **128**, 115 (2005) [*JETP* **101**, 98 (2005)].

16. V.A. Gasparov, N.S. Sidorov, and I.I. Zver'kova, *Phys. Rev.* **B73**, 094510 (2006).

17. K. Tanigaki, T.W. Ebbesen, S. Saito, J. Mizuki, J.S. Tsai, Y. Kubo, and S. Kuroshima, *Nature* (*London*) **352**, 222 (1991).

18. O. Gunnarsson, *Rev. Mod. Phys.* **69**, 575 (1997).

19. B.T. Matthias, T.H. Geballe, K. Andres, E. Corenzwit, G. Hull, and J.P. Maita, *Science* **159**, 530 (1968).

20. Y. Paderno, N. Shitsevalova, I. Batko, K. Flahbart, H. Misiorek, J. Mucha, and A. Jezowski, *J. Alloys Comp.* **219**, 215 (1995).

21. R. Lortz, Y. Wang, S. Abe, C. Meingast, Yu.B. Paderno, V. Filippov, and A. Junod, *Phys. Rev.* **B72**, 024547 (2005).

22. M. Paranthaman, C. Cantoni, H.Y. Zhai, H.M. Christen, T. Aytug, S. Sathyamurthy, E.D. Specht, J.R. Thompson, D.H. Lowndes, H.R. Kerchner, and D.K. Christen, *Appl. Phys. Lett.* **78,** 3669 (2001).

23. V.A. Gasparov and A.P. Oganesyan, *Physica* **C178**, 445 (1991).

24. A. Gauzzi, J. Le Cochec, G. Lamura, B. J. Jonsson, V.A. Gasparov, F.R. Ladan, B. Placais, P.A. Probst, D. Pavuna, and J. Bok, *Rev. Sci. Instr.* **71**, 2147 (2000).

25. V.A. Gasparov, M.R. Mkrtchyan, M.A. Obolensky, and A.V. Bondarenko, *Physica* **C1**, 197 (1994).

26. I.R. Shein and A.L. Ivanovskii, *Fiz. Tverd. Tela* (*St. Petersburg*) **45**, 1363 (2003) [*Phys. Solid State* **45**, 1429 (2003)].

27. A. Gurevich, *Phys. Rev.* **B67**, 184515 (2003).

28. B.B. Jin, N. Klein, W.N. Kang, H.-J. Kim, E.-M. Choi, S.-I. Lee, T. Dahm, K. Maki, *Phys. Rev.* **B66**, 104521 (2002).

29. L. Lyard, P. Samuely, P. Szabo, T. Klein, C. Marcenat, L. Paulius, K.H.P. Kim, C.U. Jung, H.-S. Lee, B. Kang, S. Choi, S.-I. Lee, J. Marcus, S. Blanchard, A.G. M. Jansen, U. Welp, G. Karapetrov, and W.K. Kwok, *Phys. Rev.* **B66**, R180502 (2002).

30. A.V. Sologubenko, J. Jun, S.M. Kazakov, J. Karpinski, and H.R. Ott, *Phys. Rev.* **B66**, R180505 (2002).

31. V. A. Gasparov, S.N. Ermolov, G.K. Strukova, N.S. Sidorov, S.S. Khassanov, *H*.-S. Wang, M. Schneider, E. Glaser, and Wo. Richter, *Phys. Rev.* **B63**, 174512 (2001); V.A. Gasparov, S.N. Ermolov, S.S. Khasanov, G.K. Strukova, L.V. Gasparov, *H*.-S. Wang, Qi Li, M. Schnider, Wo. Richter, E. Glaser, F. Schmidl,

P. Seidel, and B.L. Brandt, *Physica* **B284−288**, 1119 (2000).

32. A. Brinkman, A.A. Golubov, *H*. Rogalla, O.V. Dolgov, J. Kortus, Y. Kong, O. Jepsen, and O.K. Andersen, *Phys. Rev.* **B65**, R180517 (2001); A.A. Golubov, A. Brinkman, O.V. Dolgov, J. Kortus, and O. Jepsen, *Phys. Rev.* **B66**, 054524 (2002).

33. E. Helfand and N.R. Werthamer, *Phys. Rev. Lett.* **13**, 686 (1964); *Phys. Rev.* **147**, 288 (1966).